Available online at www.eccomasproceedia.org
Eccomas Proceedia COMPDYN (2025) 2162-2174

ECCOMAS
Proceedia

COMPDYN 2025
10th ECCOMAS Thematic Conference on
Computational Methods in Structural Dynamics and Earthquake Engineering
M. Papadrakakis, M. Fragiadakis (eds.)
Rhodes Island, Greece, 15-18 June 2025

INTEGRATING HEAT AND SEISMIC RISK: A MULTI-OBJECTIVE DECISION-MAKING APPROACH FOR FACADE RETROFIT DESIGN

Kyujin Kim[1], Simone D'Amore[2], Alessandra Luna-Navarro[1,], Thaleia Konstantinou[1], Mauro Overend[1], Stefano Pampanin[2], and Simona Bianchi[1]

[1] Department of Architectural Engineering and Technology, Delft University of Technology, 2628 BL Delft, The Netherlands
{K.J.Kim, T.Konstantinou, M.Overend, A.LunaNavarro, S.Bianchi }@tudelft.nl

[2] Department of Structural and Geotechnical Engineering, Sapienza University of Rome, 00184 Rome, Italy
{simone.damore, stefano.pampanin}@uniroma.it

Abstract

Current multi-hazard risk approaches in seismic engineering primarily focus on structural performance under hazards such as earthquakes, floods, and wind. Despite the distinct risk due to their direct impact on human health, heatwaves receive limited consideration. This unbalanced and fragmented approach is particularly noticeable in facade retrofit design, which has a significant influence on both structural vulnerability during earthquakes and indoor thermal conditions during heatwaves. In this case, integrating seismic and heat risk considerations would help balance performance trade-offs across both domains and assist designers in the selection and combination of technologies that are effective under seismic and heatwave conditions. This study therefore proposes a simulation-based multi-objective methodology for facade retrofit decision making. The suggested approach is demonstrated through a case study: a reinforced concrete building retrofitted using a timber rocking-dissipative external exoskeleton and precast concrete sandwich facade panels. Key facade design parameters-component capacity and dimensioning-were varied to generate a multivariate response for both seismic and thermal performance. The simulation results revealed two challenges for optimization: a limited sample size and nonlinear relationships between design inputs and performance outcomes. To address both, a multivariate regression was applied within segmented performance ranges, defined by breakpoints where the relationship between parameters and performance shifted. The resulting segmented multivariate model enabled the identification of optimal technology combinations within specific performance ranges and the generation of multiple Pareto fronts. This broadened the viable solution space and better supported project-specific trade-off decisions.

Keywords: Facade Retrofit, Heatwave Risk, Seismic Risk, Multi-objective Decision-Making, Segmented Multivariate Regression

ISSN:2623-3347
Peer-review under responsibility of the organizing committee of COMPDYN 2025.
doi: 10.7712/120125.12558.25352

1 INTRODUCTION

There is growing recognition of the need to design buildings that can withstand multiple types of extreme events, particularly in regions increasingly exposed to both seismic activity and heatwaves [1]. However, current multi-hazard risk approaches in seismic engineering primarily focus on structural performance under events such as earthquakes, floods, and wind—providing limited consideration of heatwaves. Heatwaves present a fundamentally different kind of risk: they pose an immediate threat to human health [2, 3]. Existing integrated design strategies that address seismic damage reduction alongside long-term energy efficiency [4, 5] are not sufficient for managing the short-term, acute temperature spikes characteristic of extreme heat events.

A critical point of convergence between seismic and heat risks is the building facade. Even under low-intensity earthquakes, facade damage contributes significantly to repair costs and functional disruptions [6]. During heatwaves, the envelope's thermal mass, insulation, and solar control features play a crucial role in moderating indoor temperatures and protecting occupant health [7]. The performance of facades under extreme events can be assessed using established methods: for earthquakes, the FEMA P-58 framework [8] enables facade-specific vulnerability assessments through fragility models of exterior wall components, and deriving damage and loss metrics (e.g., repair costs and time). For heatwaves, thermal comfort metrics such as Standard Effective Temperature (SET) and cumulative degree-hours of unmet SET [9] provide a means to evaluate how indoor thermal conditions for thermal safety and, indirectly, how well the facade can contribute to safe thermal conditions during periods of extreme heat with or without the presence of active cooling.

While several facade technologies have proven to be effective under either seismic [10, 11] or heatwave [12, 13] conditions, a critical gap remains in understanding how to integrate these technologies—originating from distinct domains—into a holistic facade design. Specifically, it is unclear how to identify combinations of technologies and associated design parameters that meet both seismic and heatwave performance objectives. Addressing this integration requires understanding how far a design solution can be optimized in one domain without compromising performance in another. Furthermore, there is a lack of comprehensive, pre-evaluated performance data for facade design variants. Although certain facade types and their connection properties have been experimentally tested, the resulting data is often discrete and limited to specific parametric cases. What remains unknown is how to extend these discrete results into a continuous performance range that can support performance-based design and broaden the space for optimization. This paper addresses these methodological challenges by : (1) defining how facade design parameters affect performance under both seismic and heatwave conditions, and how their trade-offs vary across different performance ranges; (2) formulating multi-objective functions to identify viable design solutions given the limited information available on specific combinations of façade technologies and their associated design parameters.

To this end, this study proposes a simulation-based workflow for integrated facade design under both seismic and heatwave hazards. The approach is demonstrated for a case study involving the retrofit of a reinforced concrete (RC) frame building, where facade design configurations are explored to reduce both seismic damage to the facade itself and unmet SET during heatwaves. A selected combination of resilient technologies is treated as design variables, and their performance is evaluated through seismic and energy simulations. Based on the resulting simulation dataset, statistical analysis is conducted to explore interrelations within this multivariate response space. This analysis informs the generation of a synthetic design samples

representing a broader range of potential design solutions. Finally, the optimal solutions from both datasets are compared to evaluate their effectiveness in revealing performance trade-offs and informing design decisions.

The paper is structured as follows. The research methodology (Section 2) outlines the selection of design parameters and their input ranges, along with the modelling and simulation workflow used to generate the initial dataset. It also describes the segmented multi-variate fitting method applied to capture the relationship between design choices and performance outcomes. The results (Section 3) present the pairwise analysis between design and performance parameters, the fitted functions across different performance levels, and the identification of integrated design cases. The conclusion (Section 4) summarizes the key findings and highlights potential directions for future research.

2 RESEARCH METHODOLOGY

2.1 Seismic and heatwave resilient design: Technologies and design variables

This study examined a retrofit scenario for a six-storey residential building in Acerra, Italy. The building was constructed in 1980s, with RC concrete beams and column frame, RC floors and hollow brick infill walls. The proposed intervention involved replacing the existing facade with a unitized cladding system to enhance its performance under seismic and heatwave conditions. Two key performance indicators are assessed: (i) damage, defined as the quantity of facade components reaching a predefined damage state under seismic loading, and (ii) unmet SET, representing discomfort hours during a heatwave.

For each performance parameter, influencing design variables were identified, including those intrinsic to the facade (e.g., connection structural capacity or insulation material), and those related to auxiliary systems (e.g., exoskeleton or shading louver) that mitigate external loads. Figure 1 shows the retrofit components and the range of design parameter variations considered in this study.

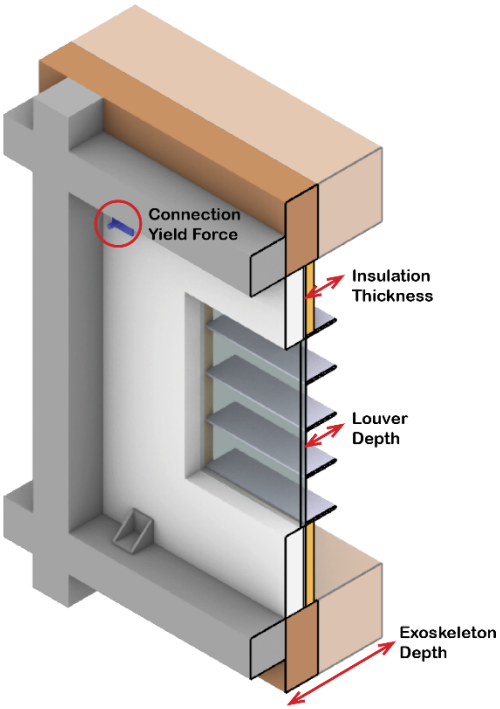

Desgin Parameter	Value
Connection Yield Force (kN)	1.9, 3.3, 9.4, 16.3, 16.9
Exoskeleton Depth (mm)	0, 320, 640, 1280, 2560
Insulation Thickness (mm)	20, 40, 60, 80 (Louver Depth = 0)
Louver Depth (mm)	0, 40, 100, 200, 300 (Insulation Thickness = 20)

→ Total Samples 5 x 5 x (4+4) = 200

Figure 1: Sectional 3D view of the assembled retrofit components and the corresponding design parameters. The variations considered for each parameter are indicated.

Connection yield force In cladding systems, the connection between the facade panel and the structural beam plays a key role in seismic performance [14]. This study employed precast concrete cladding specimen from Baird[15], using the same panel dimensions and connection components. The parametric study in Baird [15] varied the diameter (20 mm and 24 mm) and length (50 mm and 250 mm) of threaded rods, resulting in four connection configurations. The corresponding yield forces of 9.4 kN, 1.9 kN, 16.3 kN, and 3.3 kN were used in this paper as discrete design parameter values.

Exoskeleton Depth The use of timber exoskeletons has been explored as a retrofit strategy to enhance structural safety and energy performance in existing buildings [16, 17]. In particular, frame and wall systems based on Pres-Lam (Prestressed Laminated Timber) low-damage technology [18] employ a rocking and dissipative mechanism at the beam-column, column-to-foundation and wall-to-foundation connections, offering a significant enhancement in structural-seismic safety and capacity while minimizing damage to both the structural skeleton and the facade components. In this study, a timber exoskeleton utilizing Pres-Lam technology was implemented as part of the retrofit strategy. The exoskeleton was aligned with the plane of the existing reinforced concrete frame and contributes to resisting in-plane horizontal loads. The design variation was made by increasing the depth of the exoskeleton, beginning with glue laminated timber beam and column sections measuring 320 mm in width and 640 mm in height. For wider exoskeleton depth, a box-type configuration using interconnected CLT wall and slab panels was used.

Insulation Thickness Improving the insulative performance of the building envelope reduces thermal transmittance (U-value) and contributes to better indoor thermal comfort and energy efficiency [19]. For the existing hollowclay brick infill wall, the current U-value was estimated at 1.0 W/m²K, based on the use of glass wool insulation with a thermal conductivity of 0.036 W/m·K and a thickness of 20 mm. According to the Italian building energy regulation [20], the required maximum U-value for external walls is 0.4 W/m²K. To meet this standard, the insulation thickness was increased to a maximum of 80 mm, which brings the U-value down to 0.38 W/m²K. This level was considered the upper limit for retrofit, ensuring compliance with energy code requirements.

Louver Depth External shading devices reduce solar heat gains through the building envelope, improving thermal comfort and reducing cooling loads. In this study, horizontal louvers were located in front of the glazed façade area, measuring 2.72 m wide and 2.32 m high. For a south-facing façade in the Northern Hemisphere, horizontal louvers are effective in blocking high-angle summer sun while admitting lower-angle winter sun into the building. A fixed tilt angle of 45 degrees was adopted to balance shading performance and daylight access. The maximum louver depth was limited to 300 mm to avoid obstructing the occupant's view through the window.

To represent the relationship between design configurations and performance outcomes, two multivariate response functions were defined:

$$\begin{aligned} F_1 &= f_1(\textit{Connection Yield Force, Exoskeleton Depth}) && (\textit{Damage}) \\ F_2 &= f_2(\textit{Exoskeleton Depth, Insulation Thickness, Louver Depth}) && (\textit{Unmet SET}) \end{aligned} \tag{1}$$

A total of 200 design samples were generated by combining 5 values for connection yield force, 5 values for exoskeleton depth, and 8 values for either insulation thickness or louver depth (Figure 1). Insulation thickness and louver depth were not varied simultaneously; when one was varied, the other was kept constant at its baseline value.

2.2 Seismic damage

A simulation workflow was established to evaluate the seismic damage sustained by tie-back connection systems under varying connection capacities and varying exoskeleton frame dimensions. The structural model was created and analyzed using OpenSees [21, 22]. The workflow included conducting a response spectrum analysis to compute inter-storey drift values. These drift values were then combined with component fragility data to determine damage quantities using Pelicun [23], a Python library implementing the FEMA P-58 stochastic damage and loss modelling methodology [8].

Fragility curve parameters, specifically the median and dispersion values, for each tie-back configuration—defined by diameter (D) and length (L)—were sourced from Baird [15]. A fragility curve represents the probability of being or exceeding a damage state at a given lateral displacement, converted into drift by factoring in the story height. The tie-back connection system was characterized by four damage states: (1) pre-yielding, (2) post-yielding with visible cracking, (3) severe cracking, and (4) rupture of the rod. Since the structural model was elastic, the second damage state was used for evaluation. The fragility parameters, assuming the same dispersion value of 0.2, are as follows: tie-back D20 L50 had a median drift of 0.064%, tie-back D20 L250 had 0.258%, tie-back D24 L50 had 0.053%, and tie-back D24 L250 had 0.225%.

The reinforced concrete frame was modeled using elastic beam-column elements in OpenSees. C25/30 concrete, with a Young's modulus of 25 GPa, was used for cross-section measuring 300 mm width and 500 mm height. To account for the effects of concrete cracking, the second moment of area was reduced by 50% [24]. The exoskeleton structure was connected to the existing RC frame using rigid links (thus representing the effect of specifically designed dowelled connections to allow shear transfer between the RC frame and the exoskeleton), aligning nodes along the perimeter. It was modeled with GL30C glued laminated (glulam) timber [25], having a Young's modulus of 13 GPa and a shear modulus of 650 MPa. Changes in frame depth were represented by varying the cross-sectional width of exoskeleton beams and columns.

For the response spectrum analysis, the elastic response spectrum for Acerra, Italy, was used. It corresponds to the Life-Safety Limit State with a return period of 475 years and is shown in Figure 2 (a). This spectrum served as input to compute the floor displacements of the structure. Modal contributions were combined using the Complete Quadratic Combination (CQC) method [26] to calculate floor displacements and inter-storey drift ratios. Figure 2 (b) presents the inter-storey drift results for: the RC Frame alone and the RC Frame with the exoskeleton.

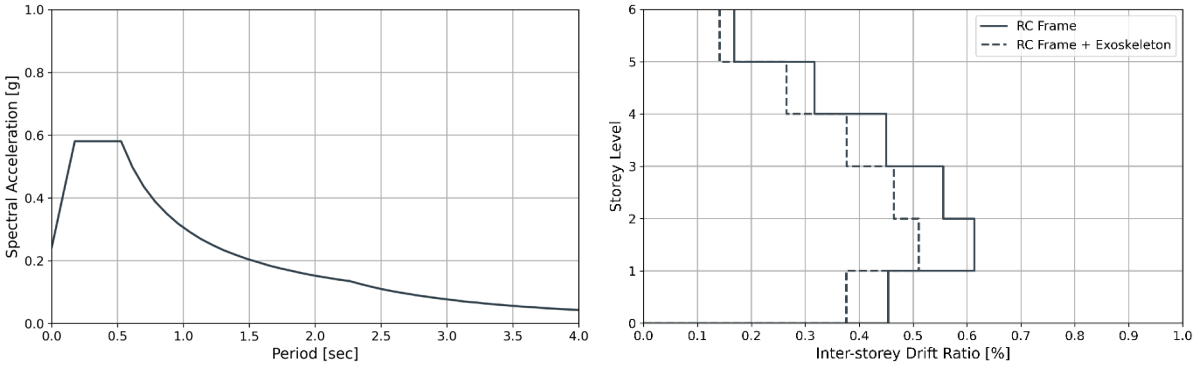

(a) (b)

Figure 2: (a) Design spectrum for Acerra, Italy, corresponding to the Life-Safety Limit state (Tr=475years) (b) Interstorey drift ratio after modal/response spetrum analysis for the RC existing as-built frame and the RC frame retrofitted with the Pres-Lam exoskeleton.

2.3 Unmet hours of safe standard effective temperatures

To assess the number of hours when thermal conditions are above safe values of SET [27] during a heatwave event, dynamic thermal simulations were conducted for varying façade configurations. Modeling was performed using the Grasshopper plugin Honeybee [28], which was exported as an IDF file for simulation in EnergyPlus [29]. From the EnergyPlus SQL output file, hourly indoor air temperature and relative humidity were extracted to compute the Standard Effective Temperature (SET) at each timestep. Cumulative unmet SET hours were calculated as the total degree-hours exceeding the comfort threshold of 30°C (SET30), in accordance with LEED Pilot Credit 129 for passive survivability [30].

In the energy model, the exoskeleton was represented as an external surface attached to the facade, providing shading and reducing solar heat gains. However, modeling it purely as an additional wall surface resulted in an overestimation of insulation due to added mass. To address this, the thermal bridge at the interface between the exoskeleton and the RC frame was accounted for by adjusting the wall's U-value. This adjustment included the effect of linear thermal transmittance (Ψ), using a reference value of 0.26 W/m·K from ASHRAE 90.1 Appendix A, which corresponds to typical balcony slab connections [31].

Historical climate data from the Open-Meteo database [32] was used to identify a representative heatwave period. The week of August 8–15, 2021 (a total of 192 hours), was selected based on daily maximum temperatures exceeding the 90th percentile for at least three consecutive days, with a peak temperature of 36.9°C. Figure 3(a) presents the outdoor dry-bulb temperature during this heatwave period, compared with the typical meteorological year. Figure 3(b) shows the cumulative unmet SET hours over the 192-hour period.

Internal loads and occupancy data were sourced from the Midrise Apartment program within the Honeybee database [28], which provides default settings of 0.025 people/m² for occupancy, 8.8 W/m² for lighting, 6.0 W/m² for equipment load, and a ventilation rate of 0.31 ACH. The building was modeled as unconditioned, with no active HVAC. Natural ventilation was implemented through operable windows, which opened when indoor air temperature exceeded 20°C and outdoor temperature remained above 15°C; otherwise, the windows remained closed.

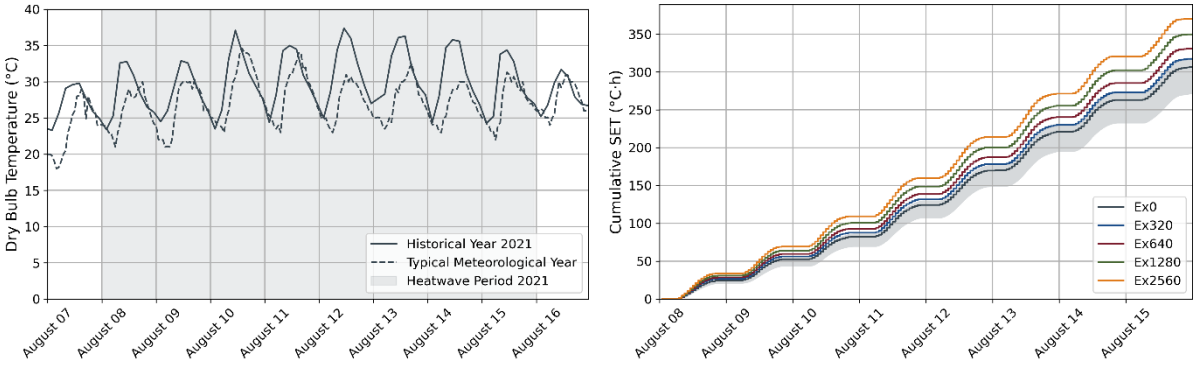

(a) (b)

Figure 3: (a) Outdoor dry-bulb temperature during the heatwave period in 2021 compared to the Typical Meteorological Year (TMY). (b) Cumulative unmet Standard Effective Temperature (SET) hours during the heatwave period, plotted for varying exoskeleton depths. For each exoskeleton (Ex) depth, the median of the sample set is shown, along with the corresponding range.

2.4 Multivariate regression analysis of seismic and thermal performance

As previously defined in the multivariate response functions, each design parameter was segmented based on detected breakpoints—locations where the trend in its relationship with the output variable (F_1 or F_2) changed. A segment approach was used to capture non-linear relationships across different input ranges rather than fitting a single global model.

For each segment combination, a local multivariate linear model was fitted, resulting in regression models that adapt to localized regions of the design space. These segmented models are defined as:

$$F_1^s = \beta_0^s + \beta_{CYF}^s \cdot Connection\ Yield\ Force + \beta_{ED}^s \cdot Exoskeleton\ Depth$$
$$F_2^t = \beta_0^t + \beta_{ED}^t \cdot Exoskeleton\ Depth + \beta_{IT}^t \cdot Insulation\ Thickness + \beta_{LD}^t \cdot Louver\ Depth \quad (2)$$

Here, s and t denote specific segment combinations for F_1 and F_2 respectively. These segmented models allow regression coefficients β to vary based on local input ranges.

Using these regression model, predicted outcomes $\widehat{F_1}$ and $\widehat{F_2}$ were generated by sampling new design combinations within the valid parameter ranges defined by the segmentation. These values were then mapped into the $\widehat{F_1}$-$\widehat{F_2}$ performance space to construct a multi-objective problem, where the objective is to minimize both $\widehat{F_1}$ and $\widehat{F_2}$, corresponding to minimal damage and minimal unmet SET, respectively.

Rather than solving this optimization analytically—which would require explicit formulations and solvers—the Pareto-optimal was estimated through a dominance-based filtering approach [33]. In this method, each predicted point is compared against all others, and a point is considered Pareto-optimal if no other point performs better in both objectives. All non-dominated points collectively form the Pareto front, representing optimal trade-offs between the two objectives. This filtering process was applied locally within each segmented output space, resulting in a set of local Pareto fronts. These localized fronts help identify high-performing solutions that are sensitive to specific design subregions.

3 RESULTS

3.1 Statistical relationships between design parameters and performance outcomes

Figure 4 presents the statistical analysis of the simulation results for the two performance parameters: damage (F_1) and unmet SET (F_2). The figure shows a pairwise matrix combining correlation and regression analyses across design parameters and performance outcomes.

The correlation coefficients in the lower-left of the matrix offer an initial view of the linear relationships among variables. Damage (F_1) shows a negative correlation with connection yield force ($r = –0.61$), indicating that greater structural robustness tends to reduce damage. Unmet SET (F_2) is positively correlated with exoskeleton depth ($r = 0.93$), indicating that deeper exoskeletons contribute to higher unmet thermal comfort hours.

The upper-right section includes scatter plots overlaid with regression curves, revealing non-linear relationships. Damage (F_1) decreases with increasing exoskeleton depth in the 0–640 mm and 1280–2560 mm ranges, while the trend reverses in the mid-range. For connection yield force, damage (F_1) reduction is more pronounced between 9.4 and 16.3 kN, indicating a steeper slope compared to the lower range. Louver depth is effective in reducing unmet SET (F_2) within the 0–100 mm range, beyond which the relationship weakens. A similar attenuation is observed with insulation thickness: unmet SET (F_2) increases slightly between 20–40 mm, but the effect fades at higher values. In both cases, the diminishing influence is likely due to the growing

dominance of exoskeleton depth, which begins to overshadow the contributions of other parameters.

The statistical analysis underscores the need to account for non-linearities and interdependencies in predictive modelling. Specifically, it calls for multivariate formulations that are sensitive to local behaviours, capturing transition points both within individual parameters and across their interactions.

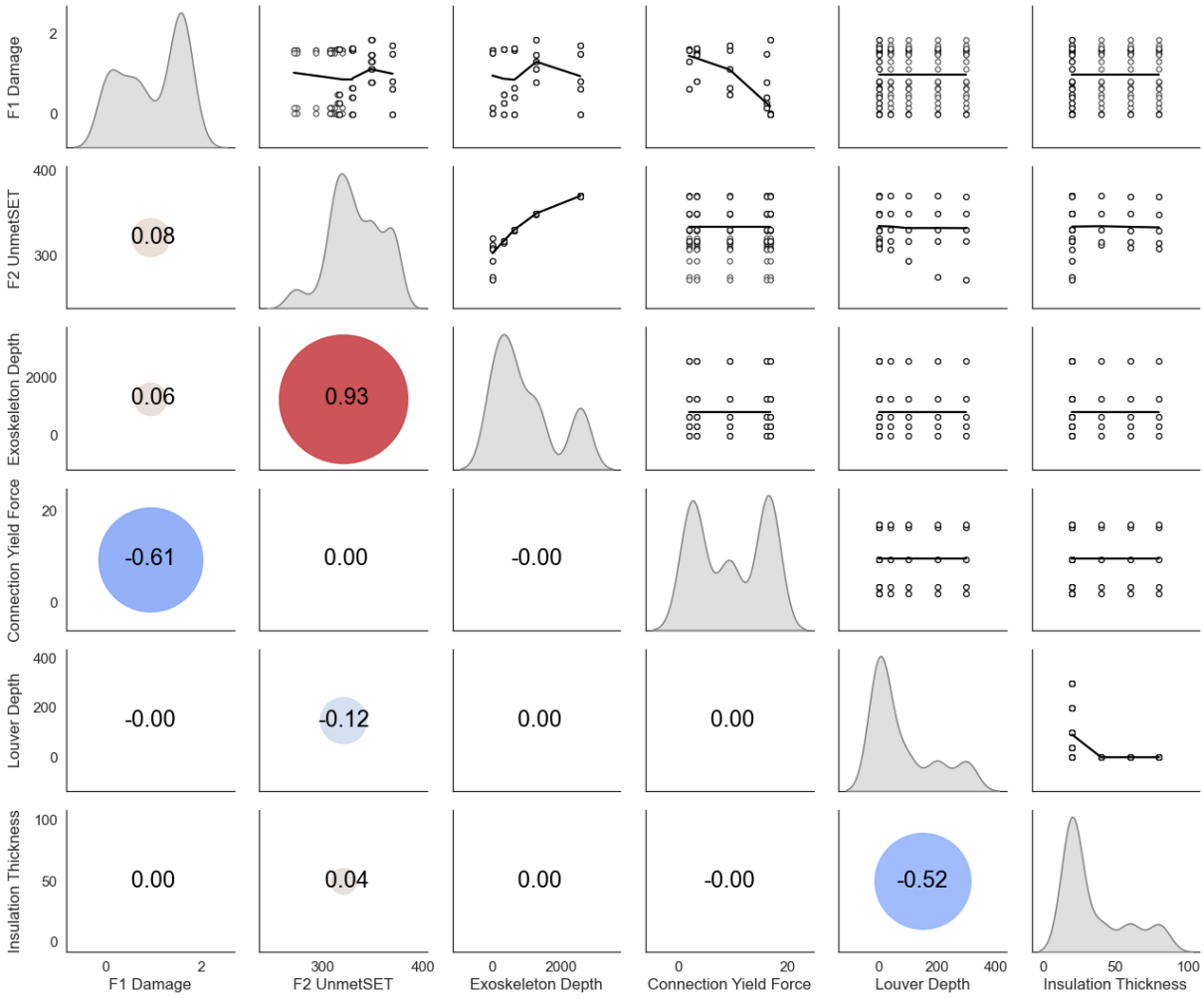

Figure 4: Pairwise relationships between design parameters and performance outcomes. The lower-left triangle shows Pearson correlation coefficients, where marker size and color reflect the strength and direction of the relationship. The diagonal shows univariate distributions, and the upper-right plots include scatter plots with locally weighted regression (LOWESS) curves.

3.2 Multivariate regression model for segmented performance ranges

Segmentation was performed for each design parameter based on detected breakpoints—locations where the trend in its relationship with the output variable (F_1 or F_2) changed. The segmented ranges for each parameter were then combined to form a gird of segments in the F_1-F_2 performance space as shown in Figure 5. The differences between the segments are, for example, seen in the transition from segment 17 to 10, which represents a reduction in damage (F_1). This change is primarily achieved by increasing the connection yield force (from a range of 1.9–15.6 kN to 14.6–16.9 kN). Similarly, moving from segment 17 to 23, which reflects a reduction in unmet SET (F_2), results from decreasing insulation thickness, while louver depth becomes irrelevant to the model.

Multivariate regression models were developed for each segment, using only the simulation data within the corresponding input parameter ranges. The regression coefficients for each fitted model are summarized in Table 1.

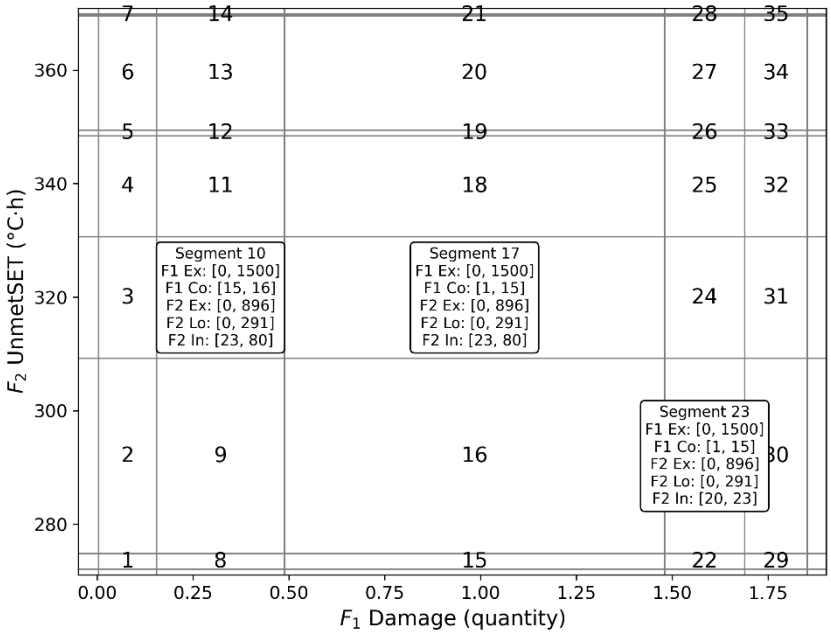

Figure 5: Segment grids overlaid on the F_1-F_2 performance space. Segment boxes are annotated with IDs and corresponding parameter ranges.

Segment	Damage (F_1)			Unmet SET (F_2)			
ID	β_{ED}	β_{CYF}	β_0	β_{ED}	β_{IT}	β_{LD}	β_0
2	0.001	0.102	-1.803	0.091	0.000	0.000	277.221
3	0.001	0.102	-1.803	0.031	-0.051	0.000	311.572
6	0.000	-2.466	41.675	0.016	0.000	-0.002	329.016
9	0.001	0.102	-1.803	0.049	0.000	-0.074	306.095
10	0.001	0.102	-1.803	0.049	0.000	-0.074	306.095
11	0.000	-0.081	1.822	0.049	0.000	-0.074	306.095
13	0.000	-2.466	41.675	0.016	-0.010	0.000	328.545
16	0.000	-0.081	1.822	0.091	0.000	0.000	277.221
17	0.000	-0.081	1.822	0.031	-0.051	0.000	311.572
18	0.001	0.102	-1.803	0.016	-0.010	0.000	328.545
19	0.001	0.102	-1.803	0.016	0.000	-0.002	329.016
20	0.000	-0.081	1.822	0.016	0.000	0.000	328.724
21	0.000	-2.466	41.675	0.016	0.000	-0.002	329.016
23	0.000	-0.081	1.822	0.091	0.000	0.000	277.221
24	0.000	-0.081	1.822	0.049	0.000	-0.074	306.095
25	0.000	-0.081	1.822	0.091	0.000	0.000	277.221
27	0.001	0.102	-1.803	0.016	-0.010	0.000	328.545
34	0.001	0.102	-1.803	0.016	0.000	0.000	328.724

Table 1: Multivariate regression coefficients for damage (F_1) and unmet SET (F_2) . Regression coefficients for design parameters are listed for each segment box.

3.3 Trade-offs in facade retrofit design decisions

Figure 6 presents scatter plots of design solutions in the F_1-F_2 performance space. Figure 6(a) shows results from simulation data, while Figure 6(b) displays newly sampled data generated using a multivariate regression model fitted to the simulation data. Within each plot, pareto optimal points are highlighted. The filtering of pareto optimal points was performed within each segment rather than across the entire dataset.

The comparison between Figure 6(a) and Figure 6(b) reveals that simulation data often yield a single local Pareto point per segment, typically aligned with the segment boundaries. In contrast, the resampled data result in a more densely populated and distributed Pareto front within each segment, providing a broader set of trade-off solutions.

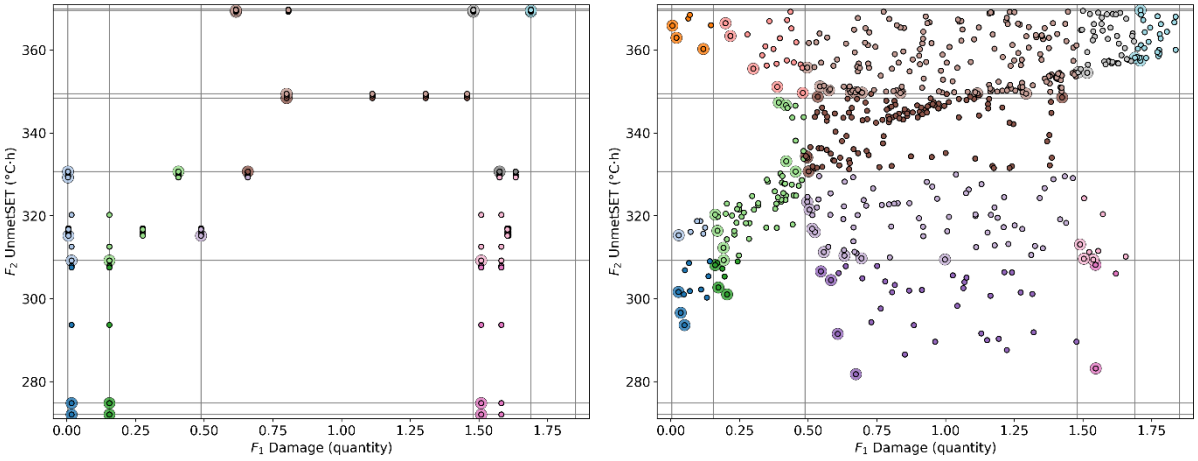

(a) (b)

Figure 6: Scatter plot of performance space damage (F_1) and unmet SET (F_2). The scatter points represent: (a) results from simulation, and (b) newly generated samples using a multivariate regression model. For each segment (refer to Figure 5), Pareto-optimal solutions are highlighted.

This expanded front enables more detailed decision-making. Table 2 summarizes the design variable values of pareto optimal solutions within segment 17 (refer to the segment numbering in Figure 5), based on the resampled datasets. No single design simultaneously achieves the lowest values for both damage (F_1) and unmet SET (F_2); instead, the Pareto front reveals the trade-offs between competing performance objectives. For example, solution 4 minimizes damage (F_1) but leads to higher unmet SET (F_2). Conversely, solution 5 reduces unmet SET (F_2) at the expense of increased damage (F_1). Solution 2 offers a more balanced option with minimal changes to design parameters, reducing the need for extensive design changes or additional resources, but with moderate performance in both damage (F_1) and unmet SET (F_2). These six solutions from the resampled datasets offer greater flexibility to accommodate project-specific priorities, in contrast to the single Pareto-optimal solution from the initial simulation dataset.

Solution ID	Performance Indicator		Design Parameters			
	Damage (quantity)	Unmet SET (°C·h)	Connection Yield Force (kN)	Exoskeleton Depth (mm)	Insulation Thickness (mm)	Louver Depth (mm)
1	0.6	310.8	14.3	460.0	26.4	241.7
2	0.5	312.2	15.5	120.8	61.4	66.8
3	0.9	310.5	11.6	75.3	66.5	184.3
4	0.5	329.1	15.9	687.4	71.7	78.2

5	1.0	310.5	9.1	334.3	27.0	162.8
6	0.5	324.9	14.9	565.5	79.1	240.2

Table 2: Pareto-optimal configurations within segment 17, showing design variable values and associated performance outcomes. The solutions are based on the resampled data from the multivariate regression model.

4 CONCLUSIONS

This study developed a simulation-based methodology to support integrated facade design under combined seismic and heatwave conditions. Key design parameters (connection capacity and façade dimensions) were assessed through seismic and thermal simulations to evaluate their impact on seismic damage and unmet thermal comfort. The simulations were based on discrete variations corresponding to specific façade component properties, which resulted in a limited dataset. To overcome this constraint and expand the solution space, multivariate regression was applied to generate synthetic design samples. Recognizing the non-linear nature of the relationships between design variables and performance outcomes, a segmented modeling approach was introduced. Within each performance segment, a localized multivariate linear model was applied. Pareto-optimal solutions were then identified from both the simulation and synthetic datasets and compared in terms of their effectiveness in supporting design decision-making.

The findings show that this approach improves informed decision-making. First, the segmented regression model accounts for variations in parameter-performance relationships across different ranges. By identifying local Pareto fronts within each segment, the method reveals which technologies are most effective under specific conditions and how their influence shifts relative to other parameters. For example, in this study on facade retrofit design using exoskeleton, tie-back connection, louver, and insulation, connection capacity was mainly correlated with seismic damage, and depth of exoskeleton with unmet thermal comfort. With this information, designers can make more targeted, context-aware decisions and better understand when and where certain strategies are most effective.

Second, the generation of a broader set of Pareto-optimal solutions from the synthetic design samples expands the range of viable design options. When performance objectives are clearly defined, the new Pareto frontiers offer design solutions that were not captured in the initial simulation results. This enables more robust performance-based design exploration, particularly in early-stage planning, where available data is often limited or discretely sampled.

This (quasi-)multi-objective methodology supports retrofit decision-making in multi-hazard contexts and addresses a key gap in integrating technologies across distinct performance domains. Future work could enhance the approach by incorporating interaction effects between the design parameters, enabling the methodology to support decisions in detailing.

Acknowledgments: This study has received funding from the European Union under the Horizon Europe Research & Innovation Programme (Grant Agreement no. 101123467 MultiCare).

REFERENCES

1. Bianchi, S.: Integrating resilience in the multi-hazard sustainable design of buildings. dpr. 2, N/A-N/A (2023). https://doi.org/10.20517/dpr.2023.16.
2. Peng, R.D., Bobb, J.F., Tebaldi, C., McDaniel, L., Bell, M.L., Dominici, F.: Toward a Quantitative Estimate of Future Heat Wave Mortality under Global Climate Change. Environmental Health Perspectives. 119, 701–706 (2011). https://doi.org/10.1289/ehp.1002430.

3. Liu, C., Kershaw, T., Fosas, D., Ramallo Gonzalez, A.P., Natarajan, S., Coley, D.A.: High resolution mapping of overheating and mortality risk. Building and Environment. 122, 1–14 (2017). https://doi.org/10.1016/j.buildenv.2017.05.028.
4. Pohoryles, D.A., Maduta, C., Bournas, D.A., Kouris, L.A.: Energy performance of existing residential buildings in Europe: A novel approach combining energy with seismic retrofitting. Energy and Buildings. 223, 110024 (2020). https://doi.org/10.1016/j.enbuild.2020.110024.
5. Pohoryles, D.A., Bournas, D.A., Da Porto, F., Caprino, A., Santarsiero, G., Triantafillou, T.: Integrated seismic and energy retrofitting of existing buildings: A state-of-the-art review. Journal of Building Engineering. 61, 105274 (2022). https://doi.org/10.1016/j.jobe.2022.105274.
6. Taghavi, S., Miranda, E.: Response Assessment of Nonstructural Building Elements, PEER Report 2003-05. Pacific Earthquake Engineering Research Center.
7. Toldi, T. de, Craig, S., Sushama, L.: Internal thermal mass for passive cooling and ventilation: adaptive comfort limits, ideal quantities, embodied carbon. Buildings & Cities. 3, (2022). https://doi.org/10.5334/bc.156.
8. FEMA: FEMA P-58-1 Seismic Performance Assessment of Buildings, Volume 1 -- Methodology, Second Edition. (2018).
9. Zhang, Y., Chen, H., Wang, J., Meng, Q.: Thermal comfort of people in the hot and humid area of China—impacts of season, climate, and thermal history. Indoor Air. 26, 820–830 (2016). https://doi.org/10.1111/ina.12256.
10. Fiorino, L., Shakeel, S., Campiche, A., Landolfo, R.: In-plane seismic behavior of lightweight steel drywall façades through quasi-static reversed cyclic tests. Thin-Walled Structures. 182, 110157 (2023). https://doi.org/10.1016/j.tws.2022.110157.
11. Baird, A., Palermo, A., Pampanin, S., Riccio, P., Tasligedik, A.S.: Focusing on reducing the earthquake damage to facade systems. Bulletin of the New Zealand Society for Earthquake Engineering. 44, 108–120 (2011). https://doi.org/10.5459/bnzsee.44.2.108-120.
12. Zhang, C., Kazanci, O.B., Levinson, R., Heiselberg, P., Olesen, B.W., Chiesa, G., Sodagar, B., Ai, Z., Selkowitz, S., Zinzi, M., Mahdavi, A., Teufl, H., Kolokotroni, M., Salvati, A., Bozonnet, E., Chtioui, F., Salagnac, P., Rahif, R., Attia, S., Lemort, V., Elnagar, E., Breesch, H., Sengupta, A., Wang, L.L., Qi, D., Stern, P., Yoon, N., Bogatu, D.-I., Rupp, R.F., Arghand, T., Javed, S., Akander, J., Hayati, A., Cehlin, M., Sayadi, S., Forghani, S., Zhang, H., Arens, E., Zhang, G.: Resilient cooling strategies – A critical review and qualitative assessment. Energy and Buildings. 251, 111312 (2021). https://doi.org/10.1016/j.enbuild.2021.111312.
13. Attia, S., Levinson, R., Ndongo, E., Holzer, P., Berk Kazanci, O., Homaei, S., Zhang, C., Olesen, B.W., Qi, D., Hamdy, M., Heiselberg, P.: Resilient cooling of buildings to protect against heat waves and power outages: Key concepts and definition. Energy and Buildings. 239, 110869 (2021). https://doi.org/10.1016/j.enbuild.2021.110869.
14. Okazaki, T., Nakashima, M., Suita, K., Matusmiya, T.: Interaction between cladding and structural frame observed in a full-scale steel building test. Earthquake Engineering & Structural Dynamics. 36, 35–53 (2007). https://doi.org/10.1002/eqe.618.
15. Baird, A.C.: Seismic Performance of Precast Concrete Cladding Systems.
16. D'Amore, S., Bianchi, S., Overend, M., Pampanin, S.: External timber-based low-damage exoskeletons for enhanced structural safety and energy efficiency. Presented at the World Conference on Earthquake Engineering (WCEE) 2024 June 30 (2024).
17. Badini, L., Ott, S., Aondio, P., Winter, S.: Seismic strengthening of existing RC buildings with external cross-laminated timber (CLT) walls hosting an integrated energetic and architectural renovation. Bull Earthquake Eng. 20, 5963–6006 (2022). https://doi.org/10.1007/s10518-022-01407-x.

18. Palermo, A., Pampanin, S., Buchanan, A., Newcombe, M.P.: Seismic Design of multi-storey buildings using laminated veneer lumber (LVL). (2005).
19. Ozel, M.: Effect of insulation location on dynamic heat-transfer characteristics of building external walls and optimization of insulation thickness. Energy and Buildings. 72, 288–295 (2014). https://doi.org/10.1016/j.enbuild.2013.11.015.
20. Lutman, F.: Decreto interministeriale 26 giugno 2015 - Applicazione delle metodologie di calcolo delle prestazioni energetiche e definizione delle prescrizioni e dei requisiti minimi degli edifici, https://www.mimit.gov.it/index.php/it/normativa/decreti-interministeriali/decreto-interministeriale-26-giugno-2015-applicazione-delle-metodologie-di-calcolo-delle-prestazioni-energetiche-e-definizione-delle-prescrizioni-e-dei-requisiti-minimi-degli-edifici.
21. Open System for Earthquake Engineering Simulation, https://opensees.berkeley.edu/.
22. openseespy: A OpenSeesPy package, https://github.com/zhuminjie/openseespy.
23. NHERI-SimCenter/pelicun, https://github.com/NHERI-SimCenter/pelicun, (2025).
24. ASCE: Seismic Evaluation and Retrofit of Existing Buildings ASCE/SEI 41-17, https://ascelibrary.org/doi/book/10.1061/9780784414859.
25. CEN, V.: EN 14080:2013 Timber structures - Glued laminated timber and glued solid timber - Requirements.
26. Chopra, A.K.: Dynamics of structure: theory and applications to earthquake engineering. Pearson/Prentice Hall, Upper Saddle River (2007).
27. Huizenga, C., Zhang, H., Schiavon, S., Kwong, H., Brager, G., Arens, E., Roa, C.D., Exss, K., Lehrer, D., Luna-Navarro, A., Nomoto, A., Ouellet-Plamondon, C., Raftery, P., Sun, R., Thero, R., Wang, Y.: Establishing Maximum Safe Indoor Temperatures for U.S. Residential Buildings. (2024).
28. Ladybug Tools LLC: Ladybug Tools | Honeybee, https://www.ladybug.tools/honeybee.html.
29. U.S. Department of Energy's (DOE): EnergyPlus, https://energyplus.net/.
30. Passive Survivability and Back-up Power During Disruptions, https://leeduser.buildinggreen.com/credit/Pilot-Credits/IPpc100, last accessed 2025/03/25.
31. ASHRAE 90.1-2022 l Energy Standard for Sites and Buildings Except Low-Rise Residential Buildings, https://www.ashrae.org/technical-resources/bookstore/standard-90-1.
32. Free Open-Source Weather API | Open-Meteo.com, https://open-meteo.com/, last accessed 2025/03/25.
33. Greco, S., Matarazzo, B., Slowinski, R.: Rough sets theory for multicriteria decision analysis. European Journal of Operational Research. 129, 1–47 (2001). https://doi.org/10.1016/S0377-2217(00)00167-3.